Tensile-stress effect on ferroelectric Barkhausen noise

Pape Jean Gueye, Hiroshi Uchida, John Edouard Blendell, Keisuke Yazawa, Benjamin Ducharne

Tensile-stress effect on ferroelectric Barkhausen noise

P.J. Gueye[1], H. Uchida[2], J.E. Blendell[3], K. Yazawa[4,5], B. Ducharne[1,6]

[1] Univ Lyon, INSA Lyon, LGEF EA682, 69621 Villeurbanne, France.
[2] Department of Materials and Life Sciences, Sophia University, Tokyo 102-8554, Japan.
[3] School of Materials Engineering, Purdue University, West Lafayette, Indiana 47907, USA.
[4] Colorado School of Mines, Golden, C0 80401, USA.
[5] National Renewable Energy Laboratory, Golden, C0 80401, USA.
[6] ELyTMaX IRL3757, Univ Lyon, INSA Lyon, Centrale Lyon, Université Claude Bernard Lyon 1, Tohoku University, Sendai 980-8577, Japan.

ABSTRACT

This study examines the effect of tensile stress on the ferroelectric properties of $Pb(Zr_{0.4}Ti_{0.6})O_3$ thin film, with a focus on Barkhausen noise, observed for the first time under such conditions. Tensile stress significantly alters domain wall motions, affecting Barkhausen noise more than average polarization. Frequency analysis identifies grain boundaries as primary pinning sites, consistent across stress levels. A non-linear relationship between stress, domain wall mobility, and polarization is found, where increased stress initially enhances pinning and polarization changes, but this effect diminishes at higher stress levels, indicating a shift in behavior.

Keywords: Ferroelectric domain switching, four-point flexural test, ferroelectric thin film, ferroelectric Barkhausen noise energy.

I - INTRODUCTION

Ferroelectric thin films are vital components in various applications, including non-volatile memory devices, sensors, actuators, and capacitors [1]. Understanding the behavior of ferroelectric thin films can lead to advancements in energy-efficient electronics and innovative solutions in data storage and processing. In ferroelectric thin films, the polarization mechanisms involve the natural alignment of electric dipoles, leading to a spontaneous polarization *P.* When an external electric field *E* is applied, the ferroelectric domains progressively align with *E*, causing domain walls to move and domains to expand in the field's direction [2]. Thickness, grain size, and substrate interaction significantly influence this reorganization [3]. Studying the kinetics of ferroelectric domains and domain wall switching in thin films is fundamental, as the speed and efficiency of domain wall switching determine the operational speed and energy consumption [4].

For the experimental data, techniques such as piezo response force microscopy (PFM, [5]) and scanning electron microscopy (SEM, [6]) are commonly used. PFM enables nanoscale visualization by applying a localized *E* via a conductive tip, while SEM, particularly when used with electron backscatter diffraction (EBSD), provides detailed imaging [7] of crystal size and domain size. Additionally, synchrotron X-ray diffraction and transmission electron microscopy (TEM) offer even higher resolution in the 10-100 nm range [8]. However, despite their advanced capabilities, these imaging techniques are costly, complex, and limited by their inability to capture the real-time dynamics of domain switching with high temporal resolution.

The origin of Barkhausen noise in ferroelectric thin films (*EBN*) lies in the discrete and abrupt movements of domain walls as they interact with defects during the polarization process [9, 10]. These motions are not smooth or continuous. Instead, domain walls get temporarily pinned by obstacles (defects, inclusion, interfaces). When the electric field is strong enough to overcome the pinning sites, the domain walls suddenly jump to a new position, causing a discrete change in polarization. These abrupt movements can be detected as current fluctuations. A detailed analysis of the *EBN* signal can infer the dynamics of domain wall motion and provide additional information where imaging techniques are limited [11].

Mechanical stress affects ferroelectric thin films by influencing the domain structure and the switching dynamic [12, 13]. Repeated stress can induce material fatigue and degrade reliability [12], while intentional strain engineering can optimize the films' properties for specific applications. Mechanical stress is predicted to influence *EBN* in thin films by altering the domain wall pinning and the dynamics of the pinning effect. Stress might increase or decrease noise intensity depending on whether it makes it easier or harder for domain walls to overcome pinning sites. However, this statement remains speculative, as to our knowledge, no experimental observations have yet provided proof of this effect.

Recently, we described the first direct measurement of Barkhausen noise in ferroelectric thin films [10]. We also proposed an innovative method to analyze ferroelectric domain wall dynamics through the reconstructed Barkhausen noise energy hysteresis cycle and its relation to the classical *P*(*E*) one. Additionally, the analysis of Barkhausen noise frequency and domain wall velocity confirmed the role of grain boundaries as dominant pinning sites in polycrystalline thin films.

In this paper, we demonstrate mechanical stress effects on the Barkhausen response and associated ferroelectric domain kinetics by leveraging the direct Barkhausen noise measurement instrument with a specific experimental setup capable of inducing a given and quasi-homogeneous traction stress to the ferroelectric thin film simultaneously in an electric field. This new setup allowed real-time monitoring of the polarization current, including the domain wall activity reflected in the *EBN*. The experimental data generated through this approach sheds light on the stress-dependent behavior of domain walls and provides a deeper understanding of the underlying mechanisms driving Barkhausen noise in ferroelectric thin films.

II – EXPERIMENTAL SETUP

2.1 Tested specimens and P(E) experimental setup

For the tested specimens, we deposited two polycrystalline $Pb(Zr_{0.4}Ti_{0.6})O_3$ (PZT) thin films (300 nm) using a chemical solution deposition method on 540 µm thick platinized silicon substrates. The precursor solution was prepared using 2-methoxyethanol, lead acetate trihydrate ($(CH_3COO)_2Pb\text{-}_3H_2O$), titanium butoxide ($Ti(O\ n\text{-}C_4H_9)_4$), and zirconium isopropoxide ($Zr(O\ i\text{-}C_3H_7)_4$). The solution was applied to the substrate through spin coating. Following the coating process, heat treatments were carried out at 150°C and 400°C for 1 minute each in air to facilitate drying and pyrolysis. For crystallization, the film underwent rapid thermal annealing at 650°C for 5 minutes in air. For x-ray diffraction spectra and detailed microstructure, refer to [14]. Circular Au top electrodes (0.1 and 0.2 mm in diameter, illustrated in Fig. S1 in Supplementary Information) were deposited during post-processing via sputtering.

We measured the stress-dependent *P*(*E*) loop using the Multiferroic II Ferroelectric Tester by RADIANT Technologies. INC. (Albuquerque, USA). This equipment captures up to 32 k points at a 2 MHz sampling rate, achieving excellent frequency resolution.

2.2 EBN characterization

To measure the *EBN*, we applied a sinusoidal voltage (5V peak-to-peak, 100Hz) to the tested specimen through a conductive point probe. We used bare surface of the PZT thin film (dark areas) (Fig. S1) for the electrical contact. This approach limited the size of measurement to the point probe surface contact (≈ 50 μm^2) and enhanced the ratio between the EBN and the low-frequency switching current [10].

Then, the induced electrical current generated was amplified and converted to a voltage signal using a Trans-Impedance Amplifier (TIA) with a feedback resistance of 10 MΩ. We set the TIA cutoff frequency near 100 kHz to avoid any Barkhausen noise filtering. We used an SDS 1104X-E scope (Siglent Technology, China) with a 1GS/s sampling rate and a record length of 14000k points per channel to capture the polarization current. Then, we used an SR650 bandpass filter (Standford Research, USA) to isolate and amplify the Barkhausen noise from the TIA's output signal. Fig. 1a depicts a schematic diagram of the experimental data acquisition chain.

2.2 Mechanical stress generation

We built a PLA 3D-printed four-point setup to induce homogeneous tensile mechanical stress to the tested specimen simultaneously with the electric field stimulus (Fig. 1b). This system was used for both the *EBN* and the *P*(*E*) characterization under applied stress.

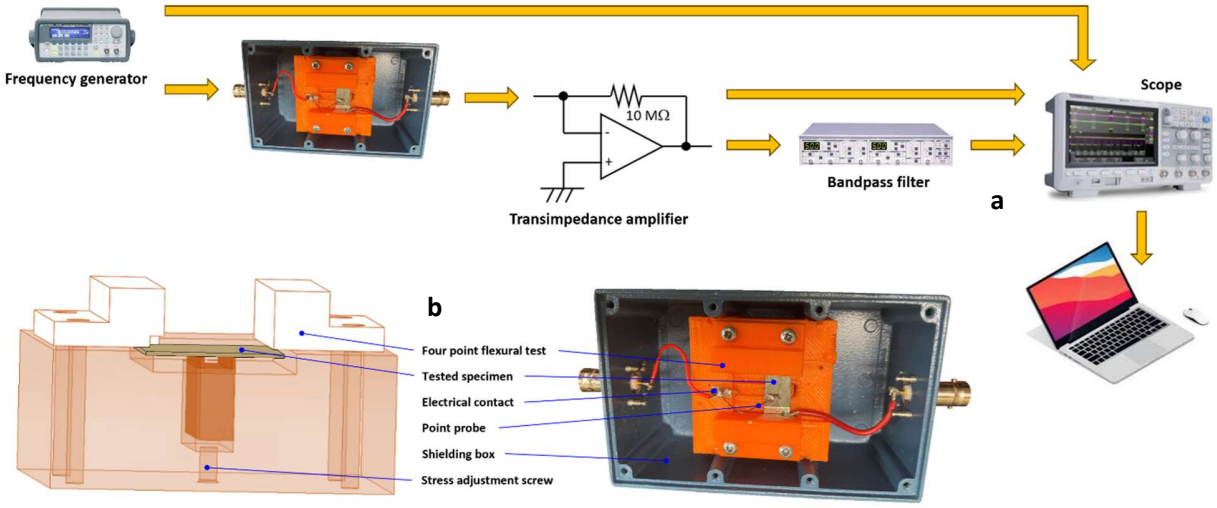

Fig. 1a – Experimental data acquisition chain **Fig. 1b –** Enlarged picture of the four-point flexural test and Barkhausen noise characterization setup.

The left and right white upper pieces in Fig. 1b clamp the tested specimen. The dark piece below the sample (in gold) translates via an adjustment screw and acts as a beam with two contact points. Together with the white pieces contacts, they form the four-point bending system, which allows a quasi-homogeneous stress between the two contact points. The deflection-load relationship of a four-point flexural test is given in Eq. 1 below:

$$\delta = \frac{P_{Load} L^3}{48EI} \tag{1}$$

$$I = \frac{bh^3}{12} \tag{2}$$

Where P_{Load} is the applied load, L is the span length between the inner supports, E is the Young modulus, I is the moment of inertia, b and h the specimen's width and thickness, respectively. Solving for P:

$$P_{Load} = \frac{4Ebh^3\delta}{L^3} \tag{3}$$

The flexural stress formula gives the tensile stress σ at the top of the specimen:

$$\sigma = \frac{3P_{Load}L}{2bh^2} \tag{4}$$

Then, substituting P from the deflection equation:

$$\sigma = \frac{6Eh\delta}{L^2} \tag{5}$$

Deflection was measured using a non-contact optical technique, where images captured by a fixed camera were analyzed to track pixel shifts at specific points on the specimen, converting these shifts into precise displacement values based on a calibrated pixel-to-length ratio.

III – EXPERIMENTAL RESULTS

3.1 Stress-depending P(E) hysteresis loop

We conducted an initial series of experimental tests to observe the effects of the in-plane tensile stress induced by the four-point flexural setup (Fig. 1b) and assess the conformity of the tested thin films. The maximum electric field amplitude was set to 1.3 10^8 $V \cdot m^{-1}$ to achieve polarization saturation, and the frequency was set to 10 kHz to minimize the influence of leakage current. Three stress levels were tested (unbent, partially bent, and fully bent), corresponding to estimated stress values of σ = 0, 20, and 80 MPa, as determined by solving Eq. 5.

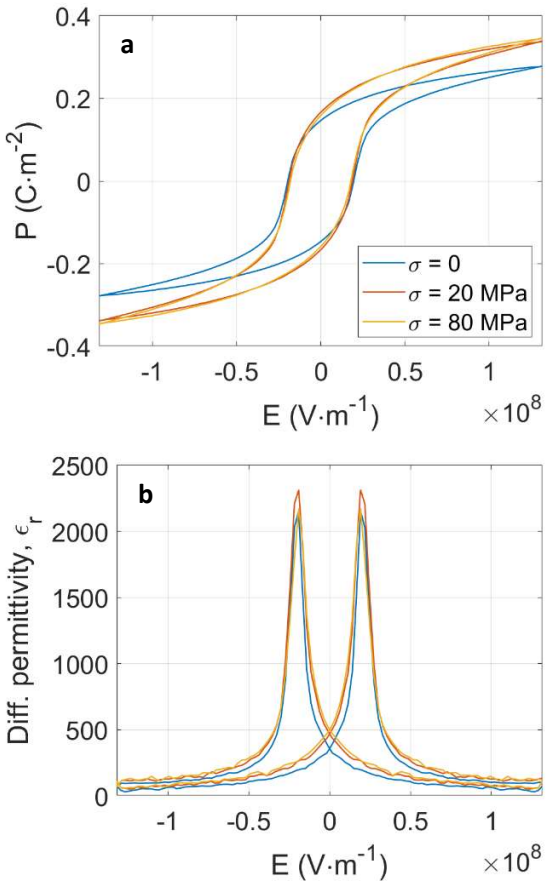

Fig. 2a – P(E) hysteresis cycles for *f* = 10 kHz σ = 0, 20, and 80 MPa **Fig. 2b –** Corresponding differential permittivity.

Mechanical stress (tensile or compressive) is known to induce changes in the shape of the P(E) hysteresis loop. Our results showed that in-plane tensile stress along the specimen's length direction increases the saturation polarization, slightly reduces coercivity, and initially enhances polarization, followed by a slight reduction between 20 and 80 MPa (Fig. 2a). An increase in differential permittivity in the cycle regions far from saturation was also observed (Fig. 2b). Similar experimental results can be seen in Fig. 5 of [15]. Although the change in polarization saturation level is smaller in [15], a similar trend is observed, confirming the reliability of the tested specimens and the experimental setup. The relatively limited difference between the *P*(*E*) loops obtained at 20 and 80 MPa could be seen as a saturation of the stress effect. This could happen when most domains have already reoriented, substrate-induced mechanical clamping limits further deformation, intrinsic material properties, defects, and grain boundaries restrict domain wall movement. However, experimental results from [11][16] show that stress keeps affecting polarization for tensile levels of 250 MPa and more, invalidating the saturation hypothesis. The effect of stress being non-linear, a large effect can happen in the low range followed by a more limited one (as observed for specimen 8 in Fig. 2 of [11]). Still, this behavior can hardly be predicted.

3.2 Stress-depending raw EBN and EBN_{energy} hysteresis cycles

We optimized the bandpass filter bandwidth (2-20 kHz) to align the *EBN* frequency and minimize the effect of the environmental noise [10]. Fig. 3 shows the filtered switching current data (red line) and the applied electric field sine wave (blue line) for each tested stress level.

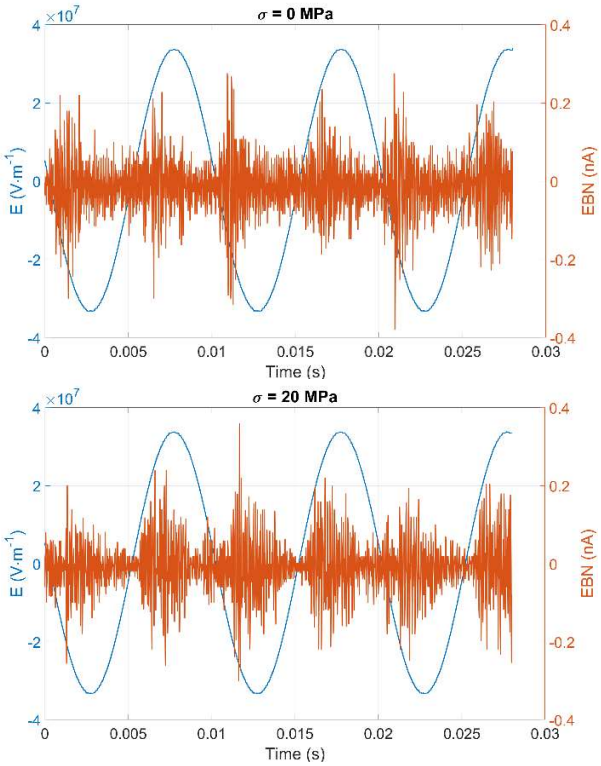

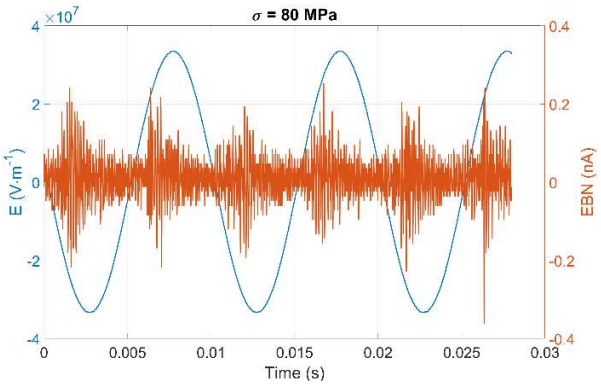

Fig. 3 – Electric field (blue) and *EBN* raw signal (red) for σ = 0, 20, and 80 MPa.

The raw *EBN* signal (Fig. 3) is stochastic and not reproducible. Therefore, it is common in the scientific community to replace it with average quantities like the RMS value [17], the envelope [18], or the so-called Barkhausen noise energy (EBN_{energy})(in ferromagnetism [19], in ferroelectricity [10]). These average indicators simplify the analysis by reducing the complexity of the raw signal, improving the signal-to-noise ratio, and providing more stable, manageable data that correlates directly with material properties. Among these indicators, we opted for the EBN_{energy} (Eq. 6) for its indirect relation to the domain wall kinetic energy [19] and the relation between the $EBN_{energy}(E)$ and the $P(E)$ cycles [10].

$$\mathrm{EBN_{energy}} = \int_0^{\mathrm{T}} \mathrm{sgn}\left(\frac{\mathrm{dE}}{\mathrm{dt}}\right) \mathrm{I_{Barkhausen}}^2 \mathrm{dt} \tag{6}$$

Fig. 4a shows the $EBN_{energy}(E)$ hysteresis cycles for σ = 0, 20, and 80 MPa after renormalization on the y-axis to ensure that all cycles have the same amplitude in the saturation zone where the EBN_{energy} is expected to be invariant. Fig. 4b displays the $P(E)$ hysteresis cycles measured in similar experimental conditions but from a deposited top electrode (Max(E) = 3.2 V·m^{-1}, f = 100 Hz). The capacitive current was removed during post-processing, and the film capacitance was estimated to be 2.43 10^{-10} F. The thin film resistance was considered high enough to neglect the leakage current.

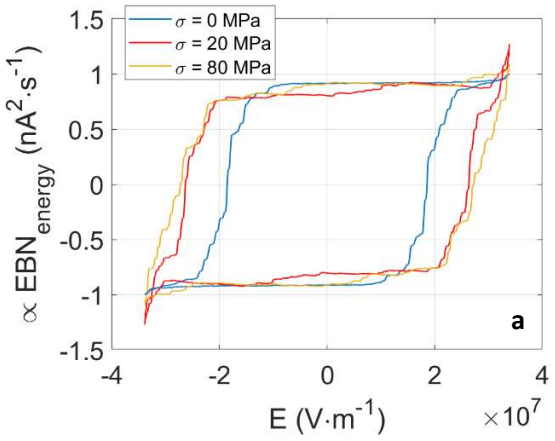

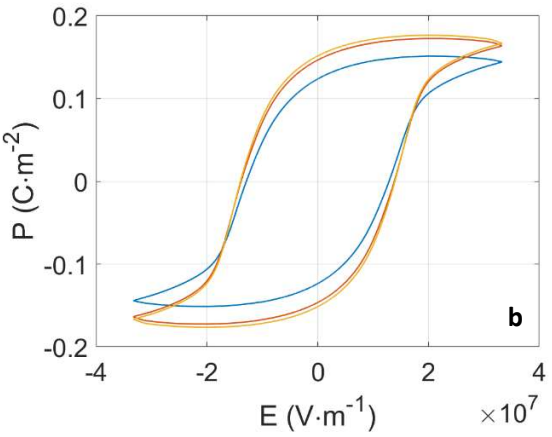

Fig. 4a – $EBN_{energy}(E)$ for σ = 0, 20, and 80 MPa **Fig. 4b –** $P(E)$ in the same experimental conditions.

The observed differences in hysteresis loop shape and coercivity between major (Fig. 2a) and minor (Fig. 4b) cycles are due to the distinct electric field ranges and measurement frequencies (10 kHz vs. 100 Hz). The hysteresis loops of Fig. 2a were taken at an electric field 6 times larger than the coercivity whereas those of Fig. 4b were measured at an electric field 2 times larger than the coercivity. The lower frequency measurement for Fig. 4b gives the lower coercivity. In addition, the leakage current contribution in Fig. 4b is associated with the low frequency measurement, which slightly curves the high-polarization zone.

IV – DISCUSSION

In [13], we combined the domain wall velocity (as described in [20]) with grain size data and demonstrated that setting the frequency bandwidth to 2–20 kHz for optimal *EBN* observations indicated that grain boundaries were the dominant domain wall pinning sites. This observation was already commented elsewhere [21]. In the present study, the same frequency bandwidth was again found to be optimal, regardless of the applied in-plane tensile stress level, confirming grain boundaries as the dominant domain wall pinning sites and stress having a limited effect on this property.

The comparison between the classical $P(E)$ loops and the $EBN_{energy}(E)$ curves reveals additional interesting observations. As illustrated in Fig. 4b, the effect of stress on the coercivity of the $P(E)$ hysteresis loops is limited. In contrast, it is significant in the $EBN_{energy}(E)$ curves (Fig. 4a). This difference in stress dependency can be attributed to several factors, including the scale at which each method operates: Barkhausen noise captures local variations, while $P(E)$ loops reflect an averaged volumetric response. Tensile stress can specifically and differently affect the local microstructure (domain wall pinning sites, defect density, etc.), leading to a distinct and local variation in coercivity. Conversely, the stress dependency in $P(E)$ loop coercivity is more associated with the overall energy landscape of domain switching, encompassing contributions from the entire ferroelectric volume.

It is also interesting to observe how the EBN_{energy} remains unchanged once the saturation elbow is surpassed while the polarization in the $P(E)$ loop continues to change up to the maximum level

of the electric field. This observation can be explained by the maximization of domain wall motion near coercivity and the polarization evolution beyond the coercive regions due to different mechanisms (ferroelectric nucleation, internal friction, dielectric relaxation, etc.). Discretizing the polarization process into different mechanisms and contributions can also justify the difference in stress dependency discussed earlier. Specifically, domain wall motions appear highly stress-dependent, with tensile stress enhancing the pinning effect and requiring higher energy to overcome natural defects. In contrast, other mechanisms are less dependent on stress.

V – CONCLUSION

In this study, we investigated the influence of tensile stress on the ferroelectric properties of a PZT thin film, with particular emphasis on Barkhausen noise, which was observed in ferroelectrics under load for the first time.

Grain boundaries were identified as the primary domain wall pinning sites, and this characteristic remained consistent across all levels of in-plane tensile stress applied.

Our analysis, conducted using both classical P(E) hysteresis loops and Barkhausen noise energy EBNenergy(E) cycles, underscored the critical role of stress in domain wall dynamics.

The results indicated that while tensile stress initially restricts domain wall mobility, leading to significant changes in the ferroelectric response, this effect diminishes at higher stress levels. Specifically, above σ = 20 MPa, the impact of stress on domain wall motion and overall ferroelectric behavior becomes limited, confirming a non-linear relationship between stress and polarization.

This study opens up several avenues for further exploration. Firstly, it is essential to confirm these observations in ferroelectric thin films with varying compositions and properties. Secondly, the impact of temperature on Barkhausen noise should be investigated. Lastly, comparing these experimental results with simulations, particularly those generated by phase field models, would be valuable in enhancing our understanding of the observed phenomena.

REFERENCES

[1] Setter, N., Damjanovic, D., Eng, L., Fox, G., Gevorgian, S., Hong, S., Kingon, A., Kohlstedt, H., Park, N.Y., Stephenson, G.B. and Stolitchnov, I., 2006. Ferroelectric thin films: Review of materials, properties, and applications. *Journal of applied physics*, *100*(5).

[2] Tagantsev, A.K., 1996. Mechanisms of polarization switching in ferroelectric thin films. *Ferroelectrics*, *184*(1), pp.79-88.

[3] Zhao, Z., Buscaglia, V., Viviani, M., Buscaglia, M.T., Mitoseriu, L., Testino, A., Nygren, M., Johnsson, M. and Nanni, P., 2004. Grain-size effects on the ferroelectric behavior of dense nanocrystalline BaTiO 3 ceramics. *Physical Review B—Condensed Matter and Materials Physics*, *70*(2), p.024107.

[4] Lang, S.B., Chan, H.L. and Shur, V.Y., 2007. Kinetics of ferroelectric domains: Application of general approach to LiNbO 3 and LiTaO 3. *Frontiers of Ferroelectricity: A Special Issue of the Journal of Materials Science*, pp.199-210.

[5] Soergel, E., 2011. Piezoresponse force microscopy (PFM). *Journal of Physics D: Applied Physics*, *44*(46), p.464003.

[6] Le Bihan, R., 1989. Study of ferroelectric and ferroelastic domain structures by scanning electron microscopy. *Ferroelectrics*, *97*(1), pp.19-46.

[7] Ihlefeld, J.F., Michael, J.R., McKenzie, B.B., Scrymgeour, D.A., Maria, J.P., Paisley, E.A. and Kitahara, A.R., 2017. Domain imaging in ferroelectric thin films via channeling-contrast backscattered electron microscopy. *Journal of Materials Science*, *52*, pp.1071-1081.

[8] Hruszkewycz, S.O., Highland, M.J., Holt, M.V., Kim, D., Folkman, C.M., Thompson, C., Tripathi, A., Stephenson, G.B., Hong, S. and Fuoss, P.H., 2013. Imaging Local Polarization in Ferroelectric Thin Films by Coherent X-Ray Bragg<? format?> Projection Ptychography. *Physical Review Letters*, *110*(17), p.177601.

[9] Tan, C.D., Gardner, J., Morrison, F.D., Salje, E.K.H. and Scott, J.F., 2018. Studies of Barkhausen Pulses in Ferroelectrics. *arXiv preprint arXiv:1805.08536*.

[10] Yazawa, K., Ducharne, B., Uchida, H., Funakubo, H. and Blendell, J.E., 2020. Barkhausen noise analysis of thin film ferroelectrics. *Applied Physics Letters*, *117*(1).

[11] Kumazawa, T., Kumagai, Y., Miura, H., Kitano, M. and Kushida, K., 1998. Effect of external stress on polarization in ferroelectric thin films. *Applied physics letters*, *72*(5), pp.608-610.

[12] Desu, S.B., 1993. Influence of stresses on the properties of ferroelectric BaTiO3 thin films. *Journal of The Electrochemical Society*, *140*(10), p.2981.

[13] Gruverman, A., Rodriguez, B.J., Kingon, A.I., Nemanich, R.J., Tagantsev, A.K., Cross, J.S. and Tsukada, M., 2003. Mechanical stress effect on imprint behavior of integrated ferroelectric capacitors. *Applied Physics Letters*, *83*(4), pp.728-730.

[14] Yazawa, K., Uchida, H. and Blendell, J.E., 2020. Origin of grain size effects on voltage-driven ferroelastic domain evolution in polycrystalline tetragonal lead zirconate titanate thin film. *Advanced Functional Materials*, *30*(9), p.1909100.

[15] Zhu, H., Chu, D.P., Fleck, N.A., Pane, I., Huber, J.E. and Natori, E., 2007. Polarization change of PZTN ferroelectric thin films under uniform in-plane tensile stress. *Integrated Ferroelectrics*, *95*(1), pp.117-127.

[16] Lim, W., Ahn, J., Kim, Y., Lee, J., Park, S.O. and Lee, S.I., 2001. The effect of stress on the electrical properties of PZT thin films. *Ferroelectrics*, *259*(1), pp.251-257.

[17] Sakamoto, H., Okada, M. and Homma, M., 1987. Theoretical analysis of Barkhausen noise in carbon steels. *IEEE transactions on magnetics*, *23*(5), pp.2236-2238.

[18] Stupakov, O., Pal'a, J., Yurchenko, V., Tomáš, I. and Bydžovský, J., 2008. Measurement of Barkhausen noise and its correlation with magnetic permeability. *Journal of magnetism and magnetic materials*, *320*(3-4), pp.204-209.

[19] Fagan, P., Ducharne, B., Daniel, L. and Skarlatos, A., 2021. Multiscale modelling of the magnetic Barkhausen noise energy cycles. *Journal of Magnetism and Magnetic Materials*, *517*, p.167395.

[20] Tybell, T., Paruch, P., Giamarchi, T. and Triscone, J.M., 2002. Domain Wall creep in epitaxial ferroelectric P b (Z r 0.2 T i 0.8) O 3 thin films. *Physical review letters*, *89*(9), p.097601.
[21] Marincel, D.M., Zhang, H., Kumar, A., Jesse, S., Kalinin, S.V., Rainforth, W.M., Reaney, I.M., Randall, C.A. and Trolier-McKinstry, S., 2014. Influence of a single grain boundary on domain wall motion in ferroelectrics. *Advanced Functional Materials*, *24*(10), pp.1409-1417.